Conquering the Dark Side: Colloidal Iron Oxide Nanoparticles

Angana Senpan,[†,∥] Shelton D. Caruthers,[†,∥] Ilsu Rhee,[†,‡] Nicholas A. Mauro,[§] Dipanjan Pan,[†] Grace Hu,[†] Michael J. Scott,[†] Ralph W. Fuhrhop,[†] Patrick J. Gaffney,[⊥] Samuel A. Wickline,[†] and Gregory M. Lanza[†,*]

[†]Department of Medicine, Washington University School of Medicine, St. Louis, Missouri 63108, [‡]Department of Physics, Kungpook National University, Daegu, Korea 702-701, [§]Department of Physics, Washington University, St. Louis, Missouri 63130, and [⊥]Department of Surgery, St. Thomas' Hospital, London, U.K. [∥]These authors contributed equally to this research project.

ABSTRACT Nanomedicine approaches to atherosclerotic disease will have significant impact on the practice and outcomes of cardiovascular medicine. Iron oxide nanoparticles have been extensively used for nontargeted and targeted imaging applications based upon highly sensitive T2* imaging properties, which typically result in negative contrast effects that can only be imaged 24 or more hours after systemic administration due to persistent blood pool interference. Although recent advances involving MR pulse sequences have converted these dark contrast voxels into bright ones, the marked delays in imaging from persistent magnetic background interference and prominent dipole blooming effects of the magnetic susceptibility remain barriers to overcome. We report a T1-weighted (T1w) theranostic colloidal iron oxide nanoparticle platform, CION, which is achieved by entrapping oleate-coated magnetite particles within a cross-linked phospholipid nanoemulsion. Contrary to expectations, this formulation decreased T2 effects thus allowing positive T1w contrast detection down to low nanomolar concentrations. CION, a vascular constrained nanoplatform administered *in vivo* permitted T1w molecular imaging 1 h after treatment without blood pool interference, although some T2 shortening effects on blood, induced by the superparamagnetic particles, persisted. Moreover, CION was shown to encapsulate antiangiogenic drugs, like fumagillin, and retained them under prolonged dissolution, suggesting significant theranostic functionality. Overall, CION is a platform technology, developed with generally recognized as safe components, that overcomes the temporal and spatial imaging challenges associated with current iron oxide nanoparticle T2 imaging agents and which has theranostic potential in vascular diseases for detecting unstable ruptured plaque or treating atherosclerotic angiogenesis.

KEYWORDS: iron oxide · molecular imaging · drug delivery · angiogenesis · ruptured plaque · MRI

Iron oxide crystals have long been used as superparamagnetic T2* contrast agents for magnetic resonance imaging (MRI).[1−4] Superparamagnetic iron oxide (SPIO, particle diameter >50 nm) and ultrasmall superparamagnetic oxide (USPIO, particle diameter <50 nm) particles have nonstoichiometric microcrystalline magnetite core(s) and are typically coated with dextran (*e.g.*, ferumoxide) or siloxane (*e.g.*, ferumoxsil).[5] At very low doses, circulating iron can decrease the T1 time of blood for positive contrast enhancement. However, at the usual doses for molecular imaging, the T2* effects predominate, resulting in short T2 relaxation with marked signal loss.[3,6,7] For molecular imaging applications, persistent T2* effects from circulating iron oxide nanoparticles delay MR imaging by 24 to 72 h post-injection.[8−10] Moreover, iron oxide nanoparticles concentrated at the target site generate dark or negative contrast with a marked blooming effect from the magnetic susceptibility artifact. Recently, new MR pulse sequences and image postprocessing techniques have been developed, which reverse the dark contrast appearance and result in a bright positive contrast effect.[11−15] Unfortunately, these techniques do not eliminate the signal loss or magnetic susceptibility artifacts, but rather exploit them to generate more easily perceived bright images of the contrast effects, often at the expense of the surrounding anatomical detail. Moreover, the undesirable 24 to 72 h delay between injection of the agent and imaging result remains. One approach to resolving the prolonged delay between treatment and imaging has been to consider the use of large SPIO particles, which clear rapidly into reticuloendothelial organs such as the liver and spleen. Such large iron oxide particles were often prone to aggregation and rapid pulmonary entrapment, and despite the leukocyte mimicking dual homing ligand approach proposed, the potential of the approach will depend on overcoming many challenges.[16−18]

Early attempts to create targeted paramagnetic contrast agents (*i.e.*, T1w bright or positive molecular imaging agents) to characterize tissues based on the presence of pathognomonic biosignatures initially failed because the payload of metal per homing unit (*e.g.*, antibody) reaching the target site was inadequate to produce detectable signal amplification. While recent peptide approaches to paramagnetic MR molecular imaging have found success

*Address correspondence to greg.lanza@mac.com.

Received for review July 17, 2009 and accepted November 6, 2009.

Published online November 12, 2009. 10.1021/nn900819y

against epitopes expressed at very high density, such as fibrin within intravascular thromboses,[19] typically nanoparticles, by virtue of their increased surface area to volume ratios and prolonged circulatory pharmacokinetics, have enjoyed the greatest success as MRI molecular imaging contrast agents. Nanoparticles benefit from higher paramagnetic metal surface payloads that rotate or tumble more slowly than small molecule organometallic compounds typically used for blood pool agents, such as Magnavist or Omniscan. Sipkins *et al.*[20] reported an $\alpha_v\beta_3$-targeted paramagnetic polymerized liposome, which was employed to detect angiogenesis in the Vx-2 tumor model 24 h after injection; some years later, a similar liposome construct was reported by Mulder *et al.* in rodent cancer models.[21−23] In a related approach, Fayad *et al.* have reported the development of paramagnetic micelles for macrophage imaging within atherosclerotic plaque.[24] We have extensively studied and reported ligand-targeted paramagnetic liquid perfluorocarbon (PFC) nanoparticles,[25−31] which have the highest reported molecular r_1 relaxivity (*i.e.*, $>$ 2 000 000 (mM (paramagnetic particles) $\cdot$ s)$^{-1}$).[28,29]

Unfortunately, recent awareness of a medical condition referred to as "nephrogenic systemic fibrosis" has created increased concern over the use of gadolinium-based contrast agents. First reports of NSF arose from a San Diego, CA hospital in a small subset of renal transplant patients who developed joint contractures, brawny induration, and hyperpigmentation of the skin in their extremities.[32] Later, this dermopathy was noted to have visceral involvement, and the early number of cases increased from the original 8 to over 250 in some registries, with all affected individuals noted to have chronic kidney disease (CKD). Clinical observation by Grobner *et al.*,[33] an Austrian nephrologist, led to the association of gadolinium-enhanced magnetic resonance angiography, which was subsequently confirmed by others.[34] The FDA issued a boxed warning stipulating that gadolinium-based contrast agents (GBCA) increased the risk for NSF in patients with chronic severe renal insufficiency, in those with acute renal insufficiency of any severity due to the hepato-renal syndrome, or in the perioperative liver transplantation period. Although prompt dialysis of patients following GBCA administration has been proposed, no evidence has suggested that hemodialysis prevents NSF.[35]

In contradistinction to blood pool agents, gadolinium chelates used for molecular imaging are typically anchored or covalently bonded to the outer surface of the nanoparticle for maximum exposure to water,[20,25,27,36,37] which alters the pharmacokinetics, biodistribution, and biological residency times *versus* current clinically approved gadolinium chelates used as blood pool agents. Although gadolinium-based molecular imaging agents have demonstrated efficacy in preclinical models, alternative non-lanthanide approaches, such as CION, are being developed and optimized while the biochemical and clinical details underlying NSF are elucidated.

Previous investigators[38,39] have reported the decrease in iron oxide T1 and T2 properties associated with intracellular encapsulation (hydrophilic matrix) *versus* freely dispersed iron oxide nanocrystals. In general, these investigators reported greater reductions in T1 than T2 relaxivity, which further increased the predominance of T2* effects over T1. In this paper, we report a unique technique wherein the encapsulation of iron oxide within a hydrophobic matrix diminished T2 effect more than T1. While the broad concept of organic ferrofluids, first reported by Bibette,[40] has known utility in many applications, this research further extends the panoply of magnetic fluid applications to MR molecular imaging.

Here we report the preparation of a novel, low magnetic susceptibility, lipid-encapsulated colloidal iron oxide nanoparticle (CION) that has high sensitivity as a T1w MRI contrast agent in conjunction with targeted drug delivery potential. Each nanoparticle core is composed of multiple polycrystalline, oleate-coated magnetite particles, suspended in vegetable oil. The

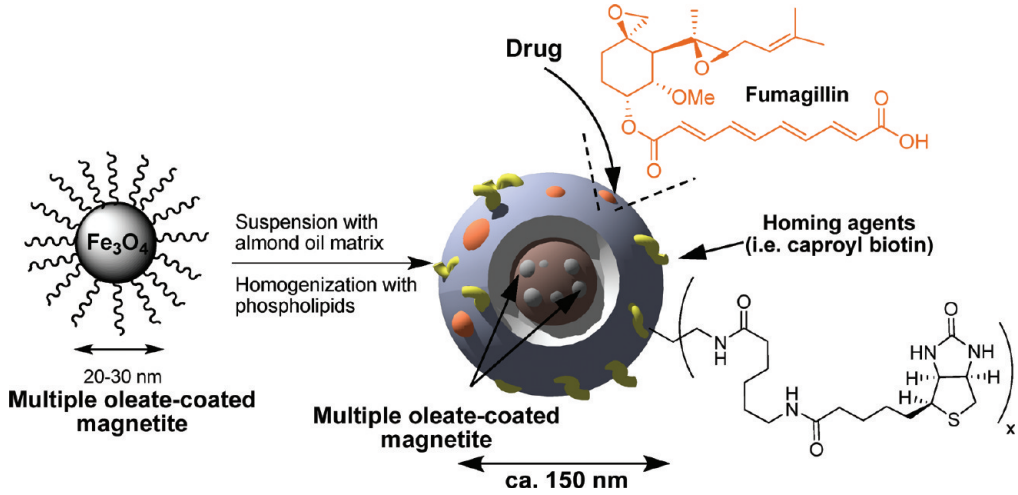

Scheme 1. Preparation of CION nanoparticles.

iron oxide/oil mixture is further encapsulated in a phospholipid monolayer through microfluidization followed by partial surfactant cross-linking. As we elaborate below, the optimized T1w imaging effect achieved was dependent on the crystalline form of iron oxide employed, the incorporated payload of iron oxide crystals within the colloid nanoparticle, and the subsequent partial cross-linking of the phospholipid surfactant. Moreover, this new agent has drug delivery potential either by dissolving or by suspending the compounds within the hydrophobic core and the encapsulating surfactant, as demonstrated for fumagillin in the present study. The phospholipid surface of CION may be functionalized to present a multiplicity of homing ligands and other imaging markers, such as fluorescent or NIR dyes to support microscopy (Scheme 1). The objective of the present study was to develop an iron-oxide-based T1w molecular imaging contrast agent that (1) permits rapid *in vivo* molecular imaging without blood pool magnetization interference, (2) minimizes typical magnetic bloom artifacts, (3) supports targeted drug delivery, and (4) is constrained to the blood pool, enhancing the specific targeting of intravascular pathology without confounding nonspecific signal from extravasated nanocolloid.

RESULTS AND DISCUSSION

Experimental colloidal iron oxide nanoparticle (CION) emulsions (20% v/v) were prepared with varying concentrations of oleic-acid-coated iron oxide (0.5, 1.0, or 3.0% [Fe] w/v) involving either magnetite (Fe_3O_4) or maghemite mixed-phase crystals (Fe_2O_3/Fe_3O_4) suspended in almond oil and encapsulated with 2% (w/v) of a phospholipid surfactant co-mixture, which was either native or partially surface cross-linked. Although other vegetable oils may be used, almond oil was selected for its high inherent abundance of oleic acid (~82%) to optimize the compatibility of the oleate-coated iron oxide.

Atomic force microscopy (AFM) of a 0.5% magnetite CION (cross-linked) revealed a particle size height$_{(av)}$ of 114 ± 22 nm and diameter$_{(av)}$ of 228 ± 69 nm; the height to width asymmetry reflecting the conformational compliance and compressibility of the CION nanoparticle against the hard AFM platform (Figure 1A). Transmission electron microscopy confirmed that the magnetite nanocrystals were exclusively retained in the oil phase rather than adhered to the outer surface or free within the hydrophilic phase (Figure 1B,C). Hydrodynamic diameter distribution for CION in aqueous suspension was determined by dynamic light scattering using a Brookhaven Instrument Co. (Holtsville, NY) Model Zeta Plus particle size analyzer. The hydrodynamic diameters of the nanocolloids without and with cross-linking were 126 ± 10 and 163 ± 10 nm, with polydispersities before and after cross-linking of 0.086 and 0.166, respectively (Figure 1D). Zeta potentials before and after cross-linking were −48 ± 5 and −23 ± 5 mV, respectively.

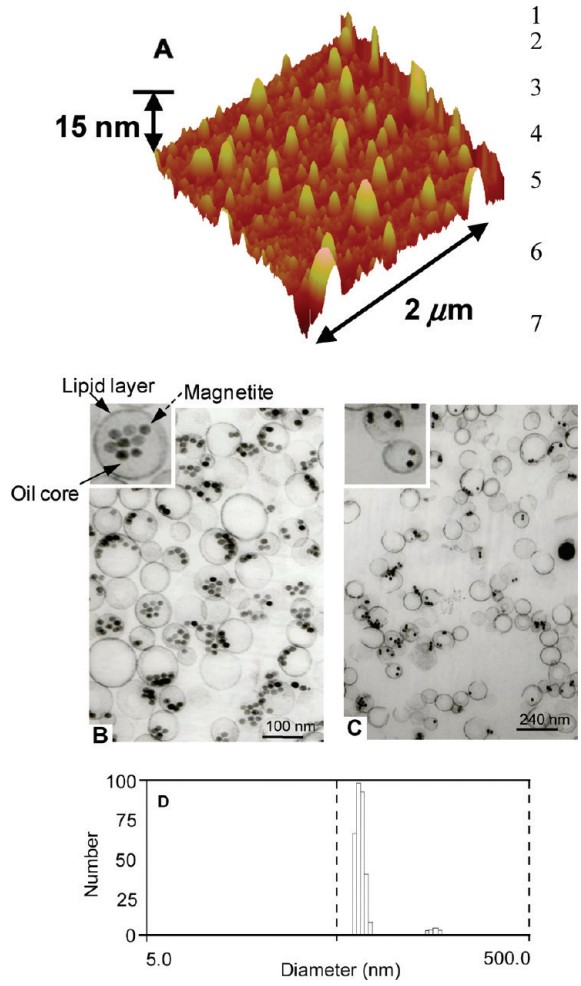

Figure 1. (A) AFM of 0.5% ([Fe] w/v) CION (H_{av} = 114 nm, D_{av} = 228 nm) reflecting high compliance of the soft particle on the hard surface. (B,C) TEM of distribution of colloidal iron oxide nanoparticles demonstrating that the oleate-coated magnetite particles are incorporated into the oil core and the core is encapsulated with lipid layer (inset B). (D) Number-averaged hydrodynamic diameter distributions of colloidal iron oxide nanoparticles.

X-ray diffraction (XRD) spectral patterns were obtained to confirm a crystal phase difference between the iron oxides used to formulate CION nanoparticles, magnetite (Fe_3O_4), and the mixed-phase maghemite (Fe_2O_3/Fe_3O_4) (Figure 2A). An XRD simulation at λ = 1.54 Å of magnetite (blue) and maghemite (green) was superimposed on the figure for illustrative reference. The X-ray diffraction pattern of the colloidal iron oxide emulsion samples was referenced to patterns derived from iron oxide powders. This textural difference was noted in the prominent reflection peak at 23.1° in mixed-phase CION. The magnetic susceptibility described by vibrating sample magnetometer (VSM) of two 0.5% iron oxide CION formulations, with and without surface cross-linking (XL), clearly revealed that the pure-phase magnetite had markedly lower magnetic properties than the mixed-phase maghemite (Figure

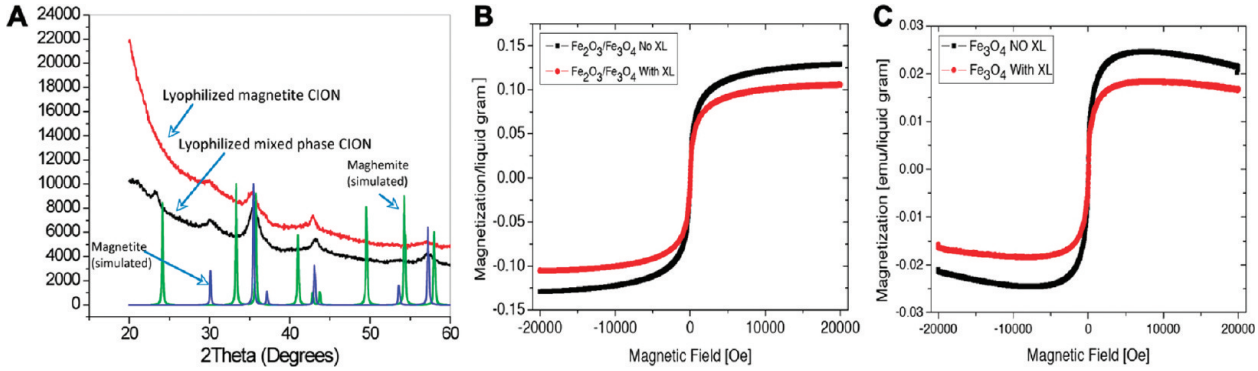

Figure 2. (A) XRD analysis of magnetite (Fe_3O_4) and mixed-phase maghemite ($Fe_2O_3-Fe_3O_4$) iron oxide crystals used for the CION nanoparticles in this study. (B) VSM magnetization (emu/liquid gram) result for mixed-phase maghemite ($Fe_2O_3-Fe_3O_4$) CION with (with XL) and without (no XL) cross-linking, which is 3 times greater than magnetite (Fe_3O_4) presented in C. Note that surfactant cross-linking consistently decreases the magnetic susceptibility of both forms of iron oxides.

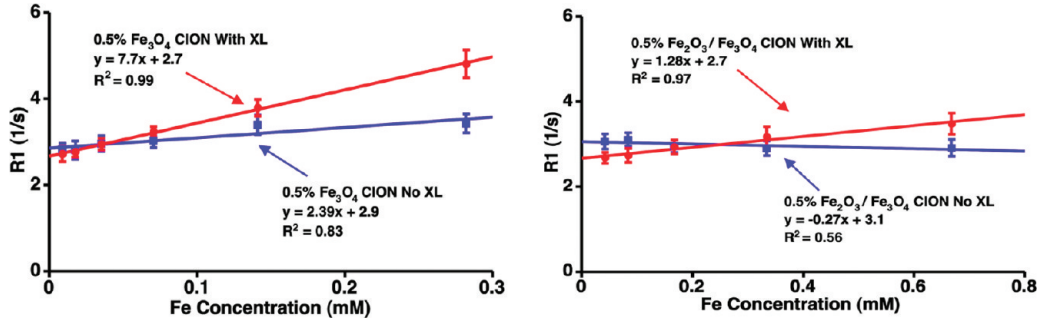

Figure 3. T1 relaxivity (r_1) of CION particles: (left) pure-phase Fe_3O_4 (magnetite); (right) $Fe_2O_3-Fe_3O_4$ (mixed-phase maghemite). The r_1 for the cross-linked, pure magnetite CION (Fe_3O_4) was 7.7 *versus* 1.3 $([Fe]mM \cdot s)^{-1}$ for $Fe_2O_3-Fe_3O_4$ (mixed-phase maghemite) CION, a 6-fold improvement associated with the lower magnetic susceptibility iron crystals.

2B,C). Moreover, cross-linking of the CION particle surfactant layers further diminished the magnetic susceptibility of both the pure- and mixed-phase CION preparations. VSM measurements of the magnetite revealed a saturation magnetic moment of 9.3×10^{-4} emu, while the remanence (sample magnetic moment after the external magnetic field at 0) was 3.4×10^{-6} emu. The strength of coercive external magnetic field required to reverse magnetic moment of the sample from saturation down to 0 was 1.519 Oersted. These negligible values of coercivity and remanent magnetization confirmed the superparamagnetic property of the magnetite but illustrated its relatively weak magnetic susceptibility.

MR properties of CION were significantly impacted by the magnetic susceptibility of the iron oxide nanocrystals, loading of iron oxide, and surface cross-linking. Pure-phase magnetite CION particles (0.5% [Fe] w/v) had higher longitudinal relaxivity (r_1) when compared with mixed-phase maghemite (Figure 3). However, increasing the iron loading of magnetite in CION from 0.5 to 3.0% ([Fe] w/v) decreased r_1. Surface cross-linking of both iron crystal forms of CION improved r_1 ($p < 0.05$). Specifically, the r_1 for the cross-linked, pure magnetite CION was 7.7 *versus* 1.3 $([Fe]mM \cdot s)^{-1}$ for $Fe_2O_3-Fe_3O_4$ (mixed-phase maghemite) CION, providing a 6-fold improvement in signal associated with the lower magnetic susceptibility cross-linked formulation (Figure 4).

Look–Locker[41] (inversion recovery) and multi-echo gradient/echo techniques were performed at 1.5 T on CION before and after cross-linking using serial dilutions

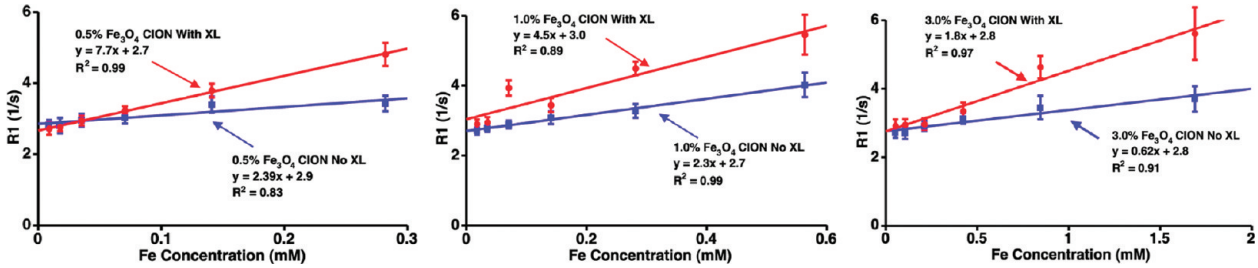

Figure 4. T1 relaxivity (r_1) of 0.5% (left), 1.0% (middle), and 3.0% (right) (w/v) magnetite (Fe_3O_4)-loaded CION. Improved relaxivity was observed with surfactant cross-linking (XL) and lower iron concentrations; *x*-axis varies due to inherent differences in [Fe].

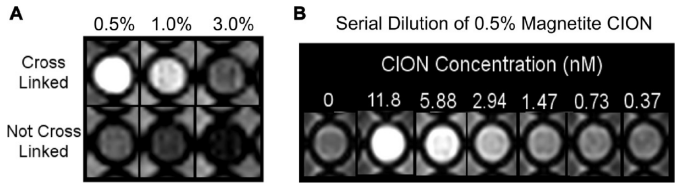

Figure 5. (A) T1w images of CION with and without surfactant cross-linking at different loadings between 0.5 and 3.0% (w/v) of magnetite in 96-well plastic dish in DI water in spaces surrounding the wells. (B) T1w-TSE image illustrates apparent, concentration-dependent, contrast with 0.5% CION at low nanomolar nanoparticle concentrations.

of 1:20 to 1:640 in plastic 96-well plates (Achieva, Philips Medical Systems, Best, The Netherlands) (Figure 5). In addition, the T1 and T2 relaxation times (ms) for magnetite CION with and without surface cross-linking at increasing iron core loadings of 0.5, 1.0, and 3.0% ([Fe] w/v) were measured. T1 relaxation times remained relatively unchanged across the 6-fold iron load range for CION independent of cross-linking. T2 relaxation time increased markedly as the iron core load decreased. T1/T2 ratios were generally lower for cross-linked magnetite CION and decreased as iron loading was reduced. Marked increases in T1w contrast of CION were clearly noted for surface cross-linked particles relative to the non-cross-linked CION (Figure 5A). Overall, the greatest T1w signal was appreciated with cross-linked, magnetite CION at the lowest iron loading used, consistent with the T1 and T2 relaxation times (Table 1). Visually obvious contrast signal (*i.e.*, T1w Turbospin Echo, T1w TSE) of 0.5% ([Fe] w/v) magnetite CION (cross-linked) serially diluted from 11.8 to 0.37 nM was appreciated into the low nanomolar particle concentration level, indicating the potential of this agent for molecular imaging of sparse biosignatures (Figure 5B).

Acellular fibrin clot phantoms were prepared and suspended on suture in saline within plastic tubes. Magnetite CION (0.5% iron, w/v, cross-linked) was targeted to the human fibrin fibrils using a highly specific monoclonal antibody and classic avidin−biotin coupling. MR TSE imaging of fibrin-targeted CION clots produced marked signal enhancement on T1w images (SNR = 26) (Figure 6B), whereas the control clot (Figure 6A) with no bound agent had a SNR = 10, similar to surrounding saline. Using T1w gradient echo, which is more sensitive than TSE to T2* decay, the contrast effect of CION was diminished relative to the T1w-TSE sequence (Figure 6C). In contradistinction to the high-resolution T1w-TSE images, T2-weighted gradient echo images of the fibrin-bound CION revealed characteristic signal dropout with magnetic susceptibility artifact blooming into many neighboring voxels (Figure 6D).

To evaluate the effectiveness of CION imaging of fibrin at pathological densities presented by human, excised human carotid endarterectomy specimens of ruptured atherosclerotic plaque were targeted with fibrin-specific magnetite CION (0.5% [Fe] w/v) using avidin−biotin coupling and imaged with MR at 3 T using T1w-TSE and gradient echo (TFE) (Figure 6E). The sharp, high-resolution "hot-spot" delineation of the fibrin deposit associated with the CEA was clearly apparent with T1w-TSE image sequences, whereas bloom artifacts and signal dropout were noted with the T1w-TFE (*i.e.*, turbo field echo) approach, consistent with the clot phantom findings presented in Figure 6. Moreover, in "typical" T2* imaging, magnetic susceptibility artifacts may be attributed to factors other than the use of iron oxide agents. For example, Figure 6E illustrates an area that is dark on both TSE and TFE, likely plaque calcium. While the positive CION signal is distinguished from such artifacts, a "typical" SPIO contrast image would be indistinguishable. These results suggest the potential of CION to provide sensitive high-resolution T1w contrast of ruptured human atherosclerotic plaque thrombus without magnetic field bloom artifacts in contradistinction to previous high spatial resolution efforts for thrombus imaging with targeted iron oxides.[42]

Although new MR imaging techniques lend themselves to positive (bright) signal contrast with iron oxide agents either by image pulse sequence or by post-processing techniques, the persistent magnetic interference from circulating nanoparticles in blood have typically required between 24 and 72 h delays between baseline imaging (*i.e.*, prior to iron oxide injection) and subsequent MR contrast-enhanced imaging. To assess the duration of magnetite CION (0.5% [Fe] w/v, cross-linked) influence on circulating whole blood relaxation times, rabbits were injected intravenously with the agent and serial blood samples were drawn over 2 h. Blood samples were accumulated and maintained under uniform conditions, then analyzed together to assess T1 and T2 properties. Whole blood T1 relaxation time following CION injection was reduced immediately but returned to baseline levels within 60 min, suggesting that MR imaging after 1 h could be performed without background blood pool contrast interference. T2 relaxivity of blood also decreased markedly after intravenous injection of CION, and a residual of this effect persisted beyond the 2 h sampling period, indicating the need for prolonged delay between iron oxide administration when performing MR T2 or T2* molecular imaging.

TABLE 1. T1 and T2 Values (ms) for CION with and without Surfactant Cross-Linking at Different Loadings (w/v) of Magnetite Using Look−Locker and CPMG Analytical Pulse Sequence Approaches, Respectively

		magnetite loading					
		0.50%		1.0%		3.0%	
	relaxation time (ms)	mean	std	mean	std	mean	std
cross-linked	T1	207.9	14.05	167.89	16.07	178.32	24.24
	T2	7.38	0.81	3.22	1.81	2.75	1.62
no cross-link	T1	291.74	18.78	248.7	21.68	270.1	27.13
	T2	8.75	2.20	4.84	3.25	2.16	0.78

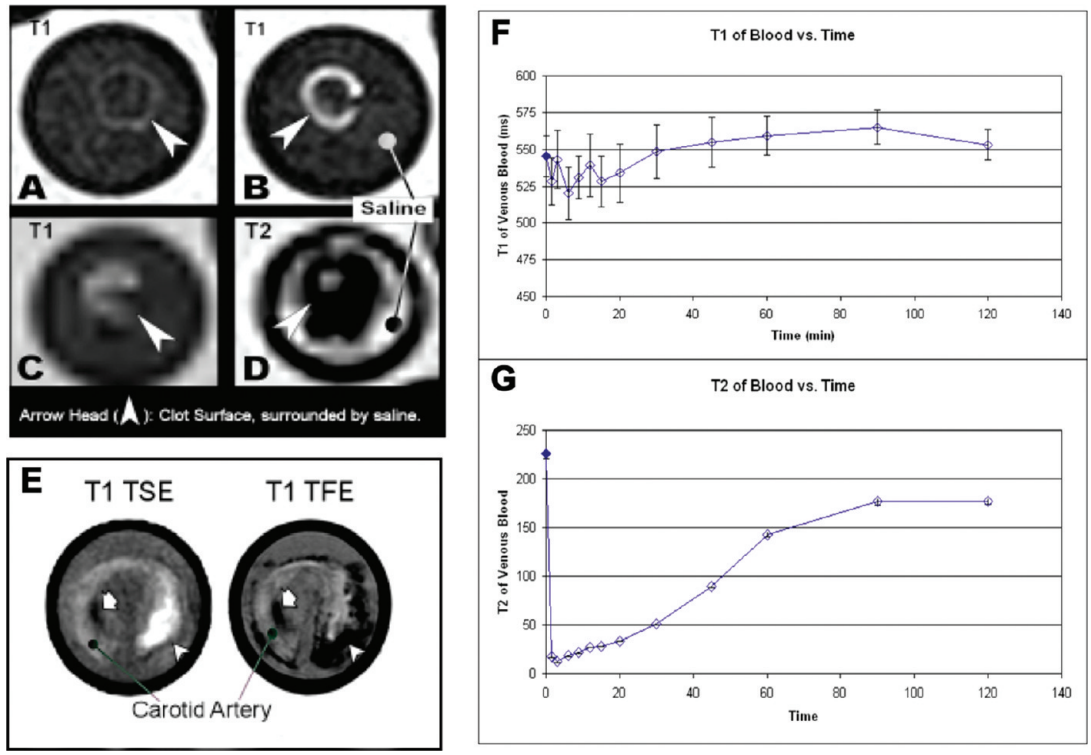

Figure 6. (A−D) Fibrin-rich clots in saline imaged at 1.5 T. (A) Control untargeted clot is not well seen on high-resolution T1w-TSE, whereas the clot with fibrin-targeted CION (B) enhances brightly. On lower resolution T1w gradient echo (FE) (C), the T1 effect is lessened, and with T2 imaging (D), the typical signal dropout effects of superparamagnetic iron oxides are pronounced, almost completely obscuring the bright signal from saline within the test tube. (The very outermost fluid is copper-sulfate-doped "phantom fluid", which is bright on both T1 and T2.) (E) Carotid endarterectomy samples targeted with CION and imaged at 3 T with bright enhancement fibrin-rich plaque on T1w-TSE, whereas gradient echo images of the same tissue (T1- and T2-weighted) displayed marked T2* effects (T1w image shown). (F,G) Dynamic T1 (F) and T2 (G) changes in blood following IV injection of CION in NZW rabbit, which show T1 background contrast due to the persistence of CION in circulation reaches preinjection levels after 1 h, whereas the T2 background contrast level persists much longer, as is expected of superparamagnetic agents imaged with T2 weighting.

Finally, nanoparticulate agents can offer both imaging and therapeutic opportunities, that is, "theranostic" agents. Some investigators have utilized iron oxide or alloy derivatives for localized hyperthermia;[43,44] others have coupled photodynamic agents to the surface for light-induced reactive oxygen species generation.[45,46] The unique design of CION permits a broad array of therapeutic options, including the targeted delivery of chemotherapeutic or antiangiogenic compounds. As previously demonstrated *in vivo*, fumagillin, a specific inhibitor of methionine aminopeptidase II, incorporated into the outer lipid membrane of lipid-encapsulated perfluorocarbon nanoparticles and targeted to the $\alpha_v\beta_3$-integrin expressed by neovascular endothelial cells can elicit a marked antiangiogenic effect in preclinical models of cancer,[47] atherosclerosis,[48,49] and rheumatoid arthritis.[50] Most nanoparticles with a chemotherapeutic payload require internalization into the target cells, and the ultimate effectiveness of therapy depends on the adequacy of endosomal escape by the bioactive drug. CION, like perfluorocarbon nanoparticles, was designed around a unique drug delivery mechanism, referred to as "contact facilitated drug delivery".[51] In this delivery approach, drugs entrapped within the outer phospholipid monolayer are transferred to the target cell following membrane hemifusion, an ATP-independent process, which is facilitated energetically by homing-ligand binding and close apposition of the particle with target cell bilayer.[52] A subsequent ATP-dependent process involving lipid rafts results in the transfer of drug into the inner bilayer leaflet and then throughout the cell lipid membrane system.[52]

In this study, we incorporated fumagillin either into the CION surfactant layer alone or in combination with core loading and measured less than 1% total release over 3 days in dissolution study against an infinite sink. These results indicate a loading efficiency of 98−99% with excellent retention in dissolution and without significant *in vitro* immediate release. A potential opportunity of the CION platform over perfluorocarbon nanoparticles may be the increased drug payload afforded by the internalization of drug within the hydrophobic core of the particle, which may act as a reservoir to load the surfactant layer when less potent compounds requiring high particle payloads are considered. A possible disadvantage for CION, however, is the requirement for partial surface cross-linking to maximize the T1w contrast imaging. Fortunately, the partial chemical cross-linking of the membrane components is esti-

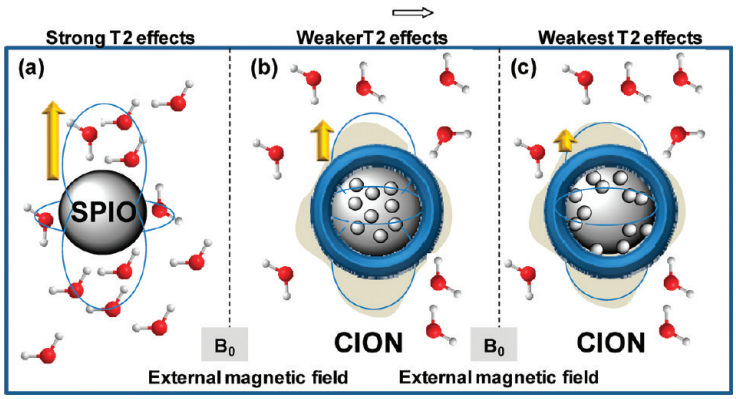

Figure 7. Cartoon illustrating hypothesis of decreased T2* effects of CION to SPIO. (a) Typical iron oxide particle surrounded by water within a B_0 field. The field-dependent dipole moment created is shown. Protons pass deep within this magnetic flux field and experience strong dephasing T2 effects. (b) Encapsulation of CION iron crystals reduces the effective field experienced by the surrounding protons, such that the relative impact on T2* is greater than the changes of T1 relaxivity. (c) Encapsulation of CION iron crystals with surfactant cross-linking further reduces the effective field experienced by the surrounding protons, such that the impact on T2* is further increased relative to the changes of T1.

mated at 10%, and the impact on membrane hemifusion and drug delivery may be trivial. Further research is required to validate drug delivery effectiveness of CION *in vivo*, but the potential is clear.

The effectiveness of CION as a T1w contrast agent was found to be dependent on lower magnetic susceptibility of pure magnetite, low core loads of metal, and chemical cross-linking of the lipid surfactant. The physical−chemical basis of the CION contrast remains to be experimentally proven, but one hypothesis is that CION encapsulation of magnetite diminished the maximum magnetic flux field influence on surrounding water (*i.e.*, protons). For normal iron oxide T2* agents, which are simply solid cores of iron, coated with or without homing ligands, water molecules pass deep into the magnetic field created by the agent within B_0 and are strongly influenced (Figure 7). For CION, suspension of 20 nm magnetite crystals in a hydrophobic core with encapsulation by a phospholipid surfactant appeared to reduce the strength of the magnetic flux experienced by surrounding protons. When the magnetic susceptibility of the iron oxide is high, such as measured for the mixed-phase maghemite particles, the magnetic influence, although lessened, remained strong and no significant T1w contrast was appreciated. However, for the magnetically weaker magnetite, lipid encapsulation further decreased the influence on surrounding water, allowing a T1w contrast effect to manifest. On the basis of the values presented in Table 1, the improvement in T1w contrast likely resulted from a proportionate lengthening of T2, which permitted the more constant T1 effects to be detected. With shorter T2, as measured for higher loads and magnetically stronger iron oxides, the T1w contrast effects were too quickly overwhelmed by the very rapid transverse decay. Cross-linking additively decreased the magnetic susceptibility of CION, but the mechanism by which chemical immobilization of the oleate-coated iron crystals improved the T1w contrast is unclear. We speculate that the oleate-coated particles may be partially cross-linked into the lipid surfactant, which may reduce closer magnetically additive interactions of individual iron oxide nanoparticles in the core of the particle induced by the B_0 magnetic field (Figure 7C). Two supportive lines of evidence for this were the TEM images (Figure 2), which suggested a greater propensity for the iron oxides to be associated with the membrane surface and less apparent in the core of the particle as appreciated in the non-cross-linked particles. Moreover, the slightly increased particle size associated with the cross-linked CION nanoparticles was paradoxical to expectation and may reflect changes in the packing density of the phospholipid molecules due to steric effects from the closely associated iron particles. Clearly further characterization, experimentation, and mathematical modeling are needed to delineate these mechanisms.

CONCLUSION

Colloidal iron oxide nanocolloid (CION) is a vascular-targeted T1w MR theranostic platform that overcomes the temporal and spatial imaging challenges associated with current iron oxide nanoparticle T2 and T2* imaging approaches. The unique MR contrast effects of CION are derived from the use of low magnetic susceptibility magnetite incorporated at low concentrations within a partially cross-linked phospholipid-encapsulated hydrophobic core nanoparticle. CION may be used to detect biosignatures present within imaging voxels at very low nanomolar densities. Illustrative examples of fibrin molecular imaging with unstable atherosclerotic plaque (*e.g.*, human carotid endarterectomy specimen) with T1w TSE demonstrated high-resolution images of thrombus without the blooming artifacts. *In vivo*, the magnetic impact on blood T1 relaxivity persisted for only 1 h, whereas T2 background effects on blood contrast persisted throughout the sampling period, which is expected of superparamagnetic iron oxide agents. Fumagillin, an antiangiogenic mycotoxin, was incorporated into CION with 98% efficiency and retained over 3 days of continuous dissolution in albumin-enriched phosphate buffer. CION offers a non-gadolinium approach to T1w MR imaging and drug therapy, with potential utility for sensitive detection of atherosclerotic ruptured plaque or antiangiogenic plaque therapy.

EXPERIMENTAL SECTION

Synthesis and Characterization of CION Nanoparticle. The colloidal iron oxide nanoparticle (CION) comprised 0.5 to 3.0% (w/v) oleate-coated iron oxide crystals (Ocean NanoTech, AR) suspended in vegetable oil, which is encapsulated by a cross-linked phospholipid-based surfactant co-mixture. The nanoparticles excipient was 1.7% (w/v) glycerin in water. Specifically, oleate-coated iron oxide was dissolved in chloroform and admixed with almond oil. Chloroform was removed under reduced pressure with mild heating (45 °C) using a rotary evaporator for 2 h.

The surfactant co-mixture included L-α-phosphatidylcholine, cholesterol, and dipalmitoylphosphatidylethanolamine (DPPE), which are dissolved in chloroform. Biotin (1.0 mol %) and/or fumagillin (0.3 mol %) were incorporated on the surface of the CION particles at the equimolar expense of L-α-phosphatidylcholine. The lipid film was resuspended in ultrapure deionized water using an ultrasonic probe (Branson Sonifier Ultrasonic Probe). Lipids, water, and iron-oxide-enriched oil were premixed into a homogeneous colloidal suspension that was transferred to a Microfluidizer S110 and homogenized at a pressure of 16 000 to 20 000 psi for 4 min. Cross-linking was performed using a bis-linker amine/acid carbodiimide coupling protocol. After processing, the nanoparticles were transferred to a sterilized 30 mL serum vial, sealed under nitrogen, and stored at 4 °C. Nanoparticle physical and chemical characterization included nominal size and zeta potential (Brookhaven Instruments, Inc.), vibration sample magnetometry, X-ray diffraction (Rigaku, Cu Kα, λ = 1.54 Å radiation), estimation of iron concentration (inductively coupled plasma mass spectrometry), atomic force microscopy (Digital 300 Series), and transmission electron microscopy (Zeiss 902).

X-ray Diffraction. X-ray diffraction scans were conducted at a scan rate of 0.1°/min using a reflection geometry of the CIONs. Colloidal iron oxide nanoparticles were lyophilized using Labconco FreeZone 4 lyophilizer, and the gel obtained from lyophilization was mounted on a glass slide for scan.

Atomic Force Microscopy. A Digital Instruments Dimension 3000 series AFM and standard Veeco tapping mode silicon probes w/Ptlr coating were used for scanning 0.5% (Fe w/v) magnetite CION. In a typical methodology, aqueous suspensions of CION samples were dried in a class 10000 clean room onto a clean glass slide for 3 h. Once dried, samples were placed on the AFM and scanned.

Transmission Electron Microscopy. Nanoparticles fixed with 2.5% glutaraldehyde (Electron Microscopy Sciences) in PBS for 30 min on ice were spun at high speed in a table top microfuge to form a tight pellet. After rinsing, the pellet was sequentially stained with osmium tetroxide, tannic acid (Sigma-Aldrich), and uranyl acetate, then dehydrated and embedded in Polybed 812 (Polysciences). Tissue was thin sectioned on a Reichert-Jung Ultracut, post-stained in uranyl acetate and lead citrate, viewed on a Zeiss 902 electron microscope, and recorded with Kodak E.M. film.

Fibrin Clot Phantoms. Fibrin clot phantoms were prepared with fresh whole porcine blood anticoagulated (9:1, v/v) with sterile sodium citrate. Plasma, retrieved post-low-speed centrifugation of the blood, was combined with 100 mmol/L calcium chloride (3:1 v/v) and 5 U thrombin (Sigma-Aldrich, Inc.) in a (low-density polyethylene) tube (~1 cc volume, i.d. ~ 6 mm). The plasma was allowed to coagulate slowly at room temperature. The clots were incubated individually with 150 μg of biotinylated antifibrin monoclonal antibody (NIB5F3)1 in 10 mL of PBS with 1% crystalline BSA (Sigma Chemical Co.) for 2 h, washed, followed by excess avidin (50 μg/mL PBS) for 30 min, washed, and then exposed to biotinylated CION (30 μL/mL PBS) for 30 min. Unbound CION was removed by further washing. Control clots were treated similarly except control oil nanoemulsions, containing no iron oxide, were substituted (30 μL/mL PBS).

MR Characterization. MR relaxation times (T1, T2, and T2*) as a function of elemental iron or CION concentrations in solution and bound to clot phantoms were determined using Look–Locker, CPMG, and multi-echo gradient echo pulse sequence approaches using 1.5 T Philips MRI. More specifically, free CION in varying serial dilutions (96-well plates) or CION bound to fibrin-rich thrombi (3 mm) suspended on suture in saline were imaged at room temperature *in vitro* within a transmit/receive quadrature birdcage head coil using a vendor-provided phantom platform with loading ring. Look–Locker sequence was used to measure T1. Specifically, a gradient echo technique with a 180° inversion prepulse followed by 45 samples (spaced by 42 ms) each with a flip angle of 14°, TE 1.9 ms, and effective TR between inversion pulses of 3.3 s with typical resolution of 0.8 × 0.8 × 6 mm^3 (320 × 315 matrix; FoV = 256 × 256 mm^2), and a total scan time of *ca.* 25 min was used. To measure T2, a CPMG-like multi-echo fast spin echo (TSE) with a 90° excitation pulse followed by multiple 180° echo train of 15 echoes separated by 4.39 ms or less with TR = 750 ms. A typical resolution of 1.0 × 1.0 × 7 mm^3 (320 × 320 matrix; FoV = 320 × 320 mm^2) required *ca.* 8 min scan time. For T2* estimates, a multi-echo gradient recalled echo technique with 32 echoes starting at 2.1 ms and separated by 3.8 ms with a flip angle of 40° and effective TR of 122 ms. Typical resolution for *in vitro* studies was 0.7 × 0.7 × 12 mm^3 (280 × 280 matrix; FoV = 196 × 196 mm^2) with an approximate scan time of 11 min. Each experimental group was replicated a minimum of three times.

T1 and T2 Pharmacokinetic Studies for CION. Two New Zealand white rabbits received CION *via* ear vein at three dosages (20% (v/v) at 1.0 mL/kg using a 0.5% magnetite loading), which corresponds roughly to 200 pmol of CION/kg. Blood sampling occurred at 0, 1, 15, 30, 45, 60, 90, and 120 min (sample temperature and O_2 were maintained constantly) to quantify the temporal change in background contrast signal. Blood samples (~1 mL/kg) were drawn from the contralateral ear from injection into tared tubes and weighed to determine aliquot volume. MR estimates of blood T1 and T2 were assessed with a Look–Locker technique[41] using 55 samples at 28 ms spacing with pixels of 1.25 × 1.25 mm^2 (matrix 216 × 213, FoV 280 × 280), flip angle = 6°, effective TR = 2.2 s, and scan time of *ca.* 12 min. For T2 blood estimates, the turbo spin echo (TSE) multi-echo technique with 20 echoes spaced 3.8 ms apart using pixels of 1.25 × 1.25 mm^2 and a TR = 900 ms was employed (1.5 T).

Kinetics of Drug Release Study by Dissolution Experiment. For dissolution studies conducted in triplicate, fumagillin CION (250 μL) was dialyzed in 60 000 molecular weight cutoff dialysis tubing against 3.5 mL of releasing medium (0.9% NaCl, 0.2 mg/mL human serum albumin, and 0.05% sodium azide) and continuously agitated at 37 °C in darkness. The releasing medium was replaced daily and analyzed for fumagillin concentration. Fumagillin was analyzed by reverse-phase HPLC (Waters Corporation) using a Waters Novapak C_{18}, 60 Å, 4 mm reversed-phase column (3.9 × 150 mm) with an isocratic 50% acetonitrile/0.05% phosphoric acid mobile phase (1 mL/min at ambient temperature).

Acknowledgment. Financial, equipment, or material support was provided by NCI, NHLBI (CA-119342 and HL094470) and Philips Healthcare and Philips Research. S.D.C., G.M.L., S.A.W., D.P., and A.S.P. are co-inventors of CION technology, which has been filed worldwide *via* PCT by Washington University Medical School.

REFERENCES AND NOTES

1. Stark, D. D.; Weissleder, R.; Elizondo, G.; Hahn, P. F.; Saini, S.; Todd, L. E.; Wittenberg, J.; Ferrucci, J. T. Superparamagnetic Iron Oxide: Clinical Application as a Contrast Agent for MR Imaging of the Liver. *Radiology* **1988**, *168*, 297–301.
2. Weissleder, R.; Hahn, P. F.; Stark, D. D.; Elizondo, G.; Saini, S.; Todd, L. E.; Wittenberg, J.; Ferrucci, J. T. Superparamagnetic Iron Oxide: Enhanced Detection of Focal Splenic Tumors with MR Imaging. *Radiology* **1988**, *169*, 399–403.
3. Frank, H.; Weissleder, R.; Brady, T. J. Enhancement of MR Angiography with Iron Oxide: Preliminary Studies in Whole-Blood Phantom and in Animals. *AJR Am. J. Roentgenol.* **1994**, *162*, 209–213.
4. Kresse, M.; Wagner, S.; Pfefferer, D.; Lawaczeck, R.; Elste, V.; Semmler, W. Targeting of Ultrasmall Superparamagnetic Iron Oxide (USPIO) Particles Tumor Cells *In Vivo* by Using Transferrin Receptor Pathways. *Magn. Reson. Med.* **1998**, *40*, 236–242.

5. Jung, C.; Jacobs, P. Physical and Chemical Properties of Superparamagnetic Iron Oxide MR Contrast Agents: Ferumoxides, Ferumoxtran, Ferumoxsil. *Magn. Reson. Imaging* **1995**, *13*, 661–674.
6. Anzai, Y.; Prince, M. R.; Chenevert, T. L.; Maki, J. H.; Londy, F.; London, M.; McLachlan, S. J. MR Angiography with an Ultrasmall Superparamagnetic Iron Oxide Blood Pool Agent. *J. Magn. Reson. Imaging* **1997**, *7*, 209–214.
7. Loubeyre, P.; Zhao, S.; Canet, E.; Abidi, H.; Benderbous, S.; Revel, D. Ultrasmall Superparamagnetic Iron Oxide Particles (AMI 227) as a Blood Pool Contrast Agent for MR Angiography: Experimental Study in Rabbits. *J. Magn. Reson. Imaging* **1997**, *7*, 958–962.
8. Schellenberger, E. A.; Bogdanov, A., Jr.; Hogemann, D.; Tait, J.; Weissleder, R.; Josephson, L. Annexin V-CLIO: A Nanoparticle for Detecting Apoptosis by MRI. *Mol. Imaging* **2002**, *1*, 102–107.
9. Kircher, M. F.; Allport, J. R.; Graves, E. E.; Love, V.; Josephson, L.; Lichtman, A. H.; Weissleder, R. *In Vivo* High Resolution Three-Dimensional Imaging of Antigen-Specific Cytotoxic T-Lymphocyte Trafficking to Tumors. *Cancer Res.* **2003**, *63*, 6838–6846.
10. Kelly, K. A.; Allport, J. R.; Tsourkas, A.; Shinde-Patil, V. R.; Josephson, L.; Weissleder, R. Detection of Vascular Adhesion Molecule-1 Expression Using a Novel Multimodal Nanoparticle. *Circ. Res.* **2005**, *96*, 327–336.
11. Cunningham, C.; Arai, T.; Yang, P.; McConnell, M.; Pauly, J.; Conolly, S. Positive Contrast Magnetic Resonance Imaging of Cells Labeled with Magnetic Nanoparticles. *Mag. Reson. Med.* **2005**, *53*, 999–1005.
12. Dharmakumar, R.; Koktzoglou, I.; Li, D. Generating Positive Contrast From Off-Resonant Spins with Steady-State Free Precession Magnetic Resonance Imaging: Theory and Proof-of-Principle Experiments. *Phys. Med. Biol.* **2006**, *51*, 4201–4215.
13. Mani, V.; Briley-Saebo, K. C.; Itskovich, V. V.; Samber, D. D.; Fayad, Z. A. Gradient Echo Acquisition For Superparamagnetic Particles With Positive Contrast (GRASP): Sequence Characterization in Membrane and Glass Superparamagnetic Iron Oxide Phantoms At 1.5T and 3T. *Magn. Reson. Med.* **2006**, *55*, 126–135.
14. Zurkiya, O.; Hu, X. Off-Resonance Saturation as a Means of Generating Contrast with Superparamagnetic Nanoparticles. *Magn. Reson. Med.* **2006**, *56*, 726–732.
15. Stuber, M.; Gilson, W. D.; Schär, M.; Kedziorek, D. A.; Hofmann, L. V.; Shah, S.; Vonken, E. J.; Bulte, J. W. M.; Kraitchman, D. L. Positive Contrast Visualization of Iron Oxide-Labeled Stem Cells Using Inversion-Recovery with On-Resonant Water Suppression (Iron). *Magn. Reson. Med.* **2007**, *58*, 1072–1077.
16. McAteer, M. A.; Sibson, N. R.; von Zur Muhlen, C.; Schneider, J. E.; Lowe, A. S.; Warrick, N.; Channon, K. M.; Anthony, D. C.; Choudhury, R. P. *In Vivo* Magnetic Resonance Imaging of Acute Brain Inflammation Using Microparticles of Iron Oxide. *Nat. Med.* **2007**, *13*, 1253–1258.
17. McAteer, M. A.; Schneider, J. E.; Ali, Z. A.; Warrick, N.; Bursill, C. A.; von zur Muhlen, C.; Greaves, D. R.; Neubauer, S.; Channon, K. M.; Choudhury, R. P. Magnetic Resonance Imaging of Endothelial Adhesion Molecules in Mouse Atherosclerosis Using Dual-Targeted Microparticles of Iron Oxide. *Arterioscler. Thromb. Vasc. Biol.* **2008**, *28*, 77–83.
18. von zur Muhlen, C.; von Elverfeldt, D.; Moeller, J. A.; Choudhury, R. P.; Paul, D.; Hagemeyer, C. E.; Olschewski, M.; Becker, A.; Neudorfer, I.; Bassler, N.; Schwarz, M.; Bode, C.; Peter, K. Magnetic Resonance Imaging Contrast Agent Targeted toward Activated Platelets Allows *In Vivo* Detection of Thrombosis and Monitoring of Thrombolysis. *Circulation* **2008**, *118*, 258–267.
19. Spuentrup, E.; Botnar, R. M.; Wiethoff, A. J.; Ibrahim, T.; Kelle, S.; Katoh, M.; Ozgun, M.; Nagel, E.; Vymazal, J.; Graham, P. B.; Gunther, R. W.; Maintz, D. MR Imaging of Thrombi Using EP-2104R, A Fibrin-Specific Contrast Agent: Initial Results in Patients. *Eur. Radiol.* **2008**, *18*, 1995–2005.
20. Sipkins, D. A.; Cheresh, D. A.; Kazemi, M. R.; Nevin, L. M.; Bednarski, M. D.; Li, K. C. Detection of Tumor Angiogenesis *In Vivo* by $\alpha_v\beta_3$-Targeted Magnetic Resonance Imaging. *Nat. Med.* **1998**, *4*, 623–626.
21. Mulder, W. J.; Strijkers, G. J.; Habets, J. W.; Bleeker, E. J.; van der Schaft, D. W.; Storm, G.; Koning, G. A.; Griffioen, A. W.; Nicolay, K. MR Molecular Imaging and Fluorescence Microscopy for Identification of Activated Tumor Endothelium Using a Bimodal Lipidic Nanoparticle. *FASEB J.* **2005**, *19*, 2008–2010.
22. Mulder, W. J.; Strijkers, G. J.; van Tilborg, G. A.; Griffioen, A. W.; Nicolay, K. Lipid-Based Nanoparticles for Contrast-Enhanced MRI and Molecular Imaging. *NMR Biomed.* **2006**, *19*, 142–164.
23. Mulder, W. J.; van der Schaft, D. W.; Hautvast, P. A.; Strijkers, G. J.; Koning, G. A.; Storm, G.; Mayo, K. H.; Griffioen, A. W.; Nicolay, K. Early *In Vivo* Assessment of Angiostatic Therapy Efficacy by Molecular MRI. *FASEB J.* **2007**, *21*, 378–383.
24. Frias, J. C.; Williams, K. J.; Fisher, E. A.; Fayad, Z. A. Recombinant HDL-like Nanoparticles: A Specific Contrast Agent for MRI of Atherosclerotic Plaques. *J. Am. Chem. Soc.* **2004**, *126*, 16316–16317.
25. Lanza, G.; Lorenz, C.; Fischer, S.; Scott, M.; Cacheris, W.; Kaufman, R.; Gaffney, P.; Wickline, S. Enhanced Detection of Thrombi with a Novel Fibrin-Targeted Magnetic Resonance Imaging Agent. *Acad. Radiol.* **1998**, *5*, s173–s176.
26. Yu, X.; Song, S.-K.; Chen, J.; Scott, M.; Fuhrhop, R.; Hall, C.; Gaffney, P.; Wickline, S.; Lanza, G. High-Resolution MRI Characterization of Human Thrombus Using a Novel Fibrin-Targeted Paramagnetic Nanoparticle Contrast Agent. *Magn. Reson. Med.* **2000**, *44*, 867–872.
27. Flacke, S.; Fischer, S.; Scott, M.; Fuhrhop, R.; Allen, J.; Mc Lean, M.; Winter, P.; Sicard, G.; Gaffney, P.; Wickline, S.; Lanza, G. A Novel MRI Contrast Agent for Molecular Imaging of Fibrin: Implications For Detecting Vulnerable Plaques. *Circulation* **2001**, *104*, 1280–1285.
28. Winter, P.; Caruthers, S.; Yu, X.; Song, S.; Fuhrhop, R.; Chen, J.; Miller, B.; Bulte, J.; Wickline, S.; Lanza, G. Improved Molecular Imaging Contrast Agent for Detection of Human Thrombus. *Magn. Reson. Med.* **2003**, *50*, 411–416.
29. Winter, P.; Athey, P.; Kiefer, G.; Gulyas, G.; Frank, K.; Fuhrhop, R.; Robertson, D.; Wickline, S.; Lanza, G. Improved Paramagnetic Chelate for Molecular Imaging with MRI. *J. Magn. Magn. Mater.* **2005**, *293*, 540–545.
30. Schmieder, A. H.; Winter, P. M.; Caruthers, S. D.; Harris, T. D.; Williams, T. A.; Allen, J. S.; Lacy, E. K.; Zhang, H.; Scott, M. J.; Hu, G.; Robertson, J. D.; Wickline, S. A.; Lanza, G. M. Molecular MR Imaging of Melanoma Angiogenesis with Alpha (V) Beta (3)-Targeted Paramagnetic Nanoparticles. *Magn. Reson. Med.* **2005**, *53*, 621–627.
31. Schmieder, A. H.; Caruthers, S. D.; Zhang, H.; Williams, T. A.; Robertson, J. D.; Wickline, S. A.; Lanza, G. M. Three-Dimensional MR Mapping of Angiogenesis with {alpha}5{beta}1({alpha}{nu}{beta}3)-Targeted Theranostic Nanoparticles in the MDA-MB-435 Xenograft Mouse Model. *FASEB J.* **2008**, *22*, 4179–4189.
32. Cowper, S. E.; Su, L. D.; Bhawan, J.; Robin, H. S.; LeBoit, P. E. Nephrogenic Fibrosing Dermopathy. *Am. J. Dermatopathol.* **2001**, *23*, 383–393.
33. Grobner, T. Gadolinium—A Specific Trigger for the Development of Nephrogenic Fibrosing Dermopathy and Nephrogenic Systemic Fibrosis. *Nephrol. Dial. Transplant.* **2006**, *21*, 1104–1108.
34. Todd, D. J.; Kagan, A.; Chibnik, L. B.; Kay, J. Cutaneous Changes of Nephrogenic Systemic Fibrosis: Predictor of Early Mortality and Association with Gadolinium Exposure. *Arthritis Rheum.* **2007**, *56*, 3433–3441.
35. Marckmann, P. An Epidemic Outbreak Of Nephrogenic Systemic Fibrosis in a Danish Hospital. *Eur. J. Radiol.* **2008**, *66*, 187–190.
36. Anderson, S. A.; Rader, R. K.; Westlin, W. F.; Null, C.; Jackson, D.; Lanza, G. M.; Wickline, S. A.; Kotyk, J. J.

Magnetic Resonance Contrast Enhancement of Neovasculature with alpha(v)beta(3)-Targeted Nanoparticles. *Magn. Reson. Med.* **2000**, *44*, 433–439.
37. Sherry, A.; Cacheris, W.; Kuan, K. Stability Constants for Gd^{3+} Binding to Model DTPA-Conjugates and DTPA-Proteins: Implications for Their Use as Magnetic Resonance Contrast Agents. *Magn. Reson. Med.* **1988**, *8*, 180–190.
38. Simon, G. H.; Bauer, J.; Saborovski, O.; Fu, Y.; Corot, C.; Wendland, M. F.; Daldrup-Link, H. E. T1 and T2 Relaxivity of Intracellular and Extracellular USPIO at 1.5T and 3T Clinical MR Scanning. *Eur. Radiol.* **2006**, *16*, 738–745.
39. Billotey, C.; Wilhelm, C.; Devaud, M.; Bacri, J. C.; Bittoun, J.; Gazeau, F. Cell Internalization of Anionic Maghemite Nanoparticles: Quantitative Effect on Magnetic Resonance Imaging. *Magn. Reson. Med.* **2003**, *49*, 646–654.
40. Bibette, J. Monodisperse Ferrofluid Emulsions. *J. Magn. Magn. Mater.* **1993**, *122*, 37–41.
41. Look, D. C.; Locker, D. R. Time Saving in Measurement of NMR and EPR Relaxation Times. *Rev. Sci. Instrum.* **1970**, *41*, 250–251.
42. Johansson, L. O.; Bjornerud, A.; Ahlstrom, H. K.; Ladd, D. L.; Fujii, D. K. A Targeted Contrast Agent for Magnetic Resonance Imaging of Thrombus: Implications of Spatial Resolution. *J. Magn. Reson. Imaging* **2001**, *13*, 615–618.
43. Kong, G.; Braun, R. D.; Dewhirst, M. W. Hyperthermia Enables Tumor-Specific Nanoparticle Delivery: Effect of Particle Size. *Cancer Res.* **2000**, *60*, 4440–4445.
44. Moroz, P.; Jones, S.; Winter, J.; Gray, B. Targeting Liver Tumors with Hyperthermia: Ferromagnetic Embolization in a Rabbit Liver Tumor Model. *J. Surg. Oncol.* **2001**, *78*, 22–29.
45. Yan, F.; Xu, H.; Anker, J.; Kopelman, R.; Ross, B.; Rehemtulla, A.; Reddy, R. Synthesis and Characterization of Silica-Embedded Iron Oxide Nanoparticles for Magnetic Resonance Imaging. *J. Nanosci. Nanotechnol.* **2004**, *4*, 72–76.
46. Lai, C. W.; Wang, Y. H.; Lai, C. H.; Yang, M. J.; Chen, C. Y.; Chou, P. T.; Chan, C. S.; Chi, Y.; Chen, Y. C.; Hsiao, J. K. Iridium-Complex-Functionalized Fe_3O_4/SiO_2 Core/Shell Nanoparticles: A Facile Three-In-One System in Magnetic Resonance Imaging, Luminescence Imaging, and Photodynamic Therapy. *Small* **2008**, *4*, 218–224.
47. Winter, P. M.; Schmieder, A. H.; Caruthers, S. D.; Keene, J. L.; Zhang, H.; Wickline, S. A.; Lanza, G. M. Minute Dosages of alpha(nu)beta3-Targeted Fumagillin Nanoparticles Impair Vx-2 Tumor Angiogenesis and Development in Rabbits. *FASEB J.* **2008**, *22*, 2758–2767.
48. Winter, P.; Caruthers, S.; Zhang, H.; Williams, T.; Wickline, S.; Lanza, G. Antiangiogenic Synergism of Integrin-Targeted Fumagillin Nanoparticles and Atorvastatin in Atherosclerosis. *J. Am. Coll. Cardiol.* **2008**, *1*, 624–634.
49. Winter, P.; Neubauer, A.; Caruthers, S.; Harris, T.; Robertson, J.; Williams, T.; Schmieder, A.; Hu, G.; Allen, J.; Lacy, E.; Wickline, S.; Lanza, G. Endothelial alpha(nu)beta(3)-Integrin Targeted Fumagillin Nanoparticles Inhibit Angiogenesis in Atherosclerosis. *Arterioscler. Thromb. Vasc. Biol.* **2006**, *26*, 2103–2109.
50. Zhou, H. F.; Chan, H. W.; Wickline, S. A.; Lanza, G. M.; Pham, C. T. $\alpha_v\beta_3$-Targeted Nanotherapy Suppresses Inflammatory Arthritis in Mice. *FASEB J.* **2009**, *23*, 2978−2985.
51. Lanza, G. M.; Yu, X.; Winter, P. M.; Abendschein, D. R.; Karukstis, K. K.; Scott, M. J.; Chinen, L. K.; Fuhrhop, R. W.; Scherrer, D. E.; Wickline, S. A. Targeted Antiproliferative Drug Delivery to Vascular Smooth Muscle Cells with a Magnetic Resonance Imaging Nanoparticle Contrast Agent: Implications for Rational Therapy of Restenosis. *Circulation* **2002**, *106*, 2842–2847.
52. Partlow, K.; Lanza, G.; Wickline, S. Exploiting Lipid Raft Transport with Membrane Targeted Nanoparticles: A Strategy for Cytosolic Drug Delivery. *Biomaterials* **2008**, *29*, 3367–3375.